Inorg. Chem. **2008**, *47*, 8306−8314

Decomposition of Dinuclear Manganese Complexes for the Preparation of Nanostructured Oxide Materials

Jonathan P. Hill,*,†,‡ Humberto Palza,§,|| Sher Alam,⊥ Katsuhiko Ariga,† Amy Lea Schumacher,# Francis D'Souza,*,# Christopher E. Anson,‡ and Annie K. Powell*,‡

Supermolecules Group and WPI-MANA, National Institute for Materials Science, 1-1 Namiki, Tsukuba, Ibaraki 305-0044, Japan, Institut für Anorganische Chemie, Universität Karlsruhe, Engesserstrasse 15, Karlsruhe, Germany D-76128, International Center for Young Scientists, National Institute for Materials Science, 1-1 Namiki, Tsukuba, Ibaraki 305-0044, Japan, Department of Chemical Engineering and Biotechnology and Centro para la Investigacion Interdisciplinaria Avanzada en Ciencias de los Materiales (CIMAT), University of Chile, Casilla 2777, Santiago, Chile, Fuel Cell Materials Group, National Institute for Materials Science (NIMS), 1-1 Namiki, Tsukuba, Ibaraki 305-0044, Japan, and Department of Chemistry, Wichita State University, 1845 Fairmount, Wichita, Kansas 67260-0051

Received May 15, 2008

The crystal structures of several dinuclear complexes of manganese are reported, and the decomposition and analysis of the nanostructured products derived from them are presented. 1,4,7,10-Tetraazacyclododecane (cyclen) forms dinuclear complexes **1**−**4** containing doubly oxo-bridged or oxo−acetato bridging ligands depending on the manganese salt used for the reaction. Doubly oxo-bridged **1** crystallizes in the orthorhombic space group *Pnma*, $a = 22.3850(14)$ Å, $b = 9.1934(5)$ Å, $c = 13.2424(10)$ Å, $V = 2725.2(3)$ Å^3. **2**, containing $[Mn(SCN)_5]^{3-}$ conteranions, crystallizes in monoclinic space group *I*2/*a* with $a = 18.2699(10)$ Å, $b = 11.2384(6)$ Å, $c = 18.6432(9)$ Å, $\alpha = 90.00°$, $\beta = 114.510(6)°$, $\gamma = 90.00°$, $V = 3483.0(3)$ Å^3. Oxo−acetato-bridged **3** crystallizes in orthorhombic space group *Pca*21, $a = 13.9322(11)$ Å, $b = 16.2332(13)$ Å, $c = 14.6794(8)$ Å, $V = 3320.0(4)$ Å^3. Compound **4** consists of a templated quasi-one-dimensional manganese oxalate crystallized in the triclinic space group $P\bar{1}$, $a = 9.5442(11)$ Å, $b = 10.3758(10)$ Å, $c = 21.851(2)$ Å, $\alpha = 83.720(12)°$, $\beta = 80.106(13)°$, $\gamma = 85.457(13)°$, $V = 2114.9(4)$ Å^3. Compounds **1**, **3**, and **4** decompose to nanostructured oxide materials, which may be isolated in bulk as lamellar-structured particles or microspheres or deposited on substrates.

Introduction

Dinuclear complexes of medium-valent manganese cations bridged through oxo ligands have long been considered for their potential as models of manganese-containing enzymes.[1] Polynuclear complexes of manganese also compose a substantial subfamily of the molecular magnets.[2] Additionally, coordination complexes of manganese have frequently been employed as precursors in the synthesis of a variety of oxide materials of industrial, technological, or academic importance.[3] There are many examples of acetato- and/or oxo-bridged dinuclear complexes of manganese with various ligands. Fortunately, the subject has been covered comprehensively by a recent review.[4] Several morphologies of nanostructured manganese oxides have been previously

* To whom correspondence should be addressed. E-mail: Jonathan.Hill@nims.go.jp (J.P.H.), francis.dsouza@wichita.edu (F.D.), powell@aoc.uni-karlsruhe.de (A.K.P.). Phone: +81-29-860-4399 (J.P.H.), +49-721-608-2135 (A.K.P.). Fax: +81-29-860-4832 (J.P.H.).

† Supermolecules Group and WPI-MANA, National Institute for Materials Science.

‡ Universität Karlsruhe.

§ International Center for Young Scientists, National Institute for Materials Science.

|| University of Chile.

⊥ Fuel Cell Materials Group, National Institute for Materials Science.

Wichita State University.

(1) (a) *Manganese Redox Enzymes*; Pecoraro, V. L., Ed.; VCH: New York, 1992. (b) Dismukes, C. G. *Chem. Rev.* **1996**, *96*, 2909–2926. (c) Kessissoglou, D. P. *Manganese−Proteins and Enzymes and Relevant Trinuclear Synthetic Complexes*; Kluwer: Dordrecht, The Netherlands, 1995.

(2) For example, see: (a) Lis, T. *Acta Crystallogr., Sect. B* **1980**, *36*, 2042–2046. (b) Hill, S.; Edwards, R. S.; Aliaga-Alcalde, N.; Christou, G. *Science* **2003**, *302*, 1015–1018. (c) Ako, A. M.; Hewitt, I. J.; Mereacre, V.; Clérac, R.; Wernsdorfer, W.; Anson, C. E.; Powell, A. K. *Angew. Chem., Int Ed.* **2006**, *45*, 4926–4929.

10.1021/ic8008915 CCC: $40.75
Published on Web 08/07/2008

reported including nanoparticles,[5] nanosheets,[6] hollow nanoshells,[7] nanofibers,[8] or mesoporous materials,[9] while a microspherical form containing a lamellar internal nanostructure has recently been reported.[10] Such structures have potential in electro- and photochemical devices.[11]

In this work, we examined the case of dinuclear manganese complexes with a tetraazamacrocyclic ligand. These are interesting from a supramolecular point of view because they have the potential to act as hydrogen-bond donors at eight sites within the molecule and can also exist in a variety of oxidation states. The latter is important because changing the oxidation state provides a means for variation of the multiplicity of counterions present upon crystallization. The N_4-donor ligand 1,4,7,10-tetraazacyclododecane (cyclen) was selected for its ability to stabilize the medium (3+ and 4+) oxidation states of manganese. The complexes can exist in a variety of packing motifs within their crystals, in which they can exhibit some reversible redox activity and in which multiple hydrogen-bond donation can stabilize extended structures including a quasi-one-dimensional manganese(II) oxalate. While the dinuclear unit can behave as a supramolecular tecton or template, the templated oxalate can behave as a precursor for micro- and nanostructured materials. Also, during our work toward obtaining the nanostructured products in a film form for use in a variety of devices, we found a novel "peel-back" method for fabrication of immobilized micron-thickness films of the hybrid materials.

Results and Discussion

The structures of the dinuclear complexes studied in this work are shown in Figure 1. The compounds were prepared by reactions between cyclen and the respective manganese salts (+ coreactant): manganese(II) chloride ($NaClO_4$; **1**), manganese(II) chloride (NaNCS; **2**), manganese(II) acetate ($NaClO_4$; **3**), or manganese(II) oxalate (**4**). The dinuclear units of compounds **1**, **2**, and **4** have identical compositions including a di-μ-oxo-bridged $Mn^{III}Mn^{IV}$ core. The important difference between the states of this dinuclear unit lies in the conformations of the amine hydrogen-bond-donating groups, as illustrated in Figure 1a,c. In **1**, hydrogen bonding with chloride counteranions leads to an extended corrugated sheet structure,[10] while for **2**, a network structure results from hydrogen bonding. In **4**, a similar interaction is responsible for templating a chainlike manganese(II) oxalate (see below). The variation in hydrogen-bonding interactions within the crystals has a significant effect on the conformation of the cyclen macrocycles even though they are constrained by

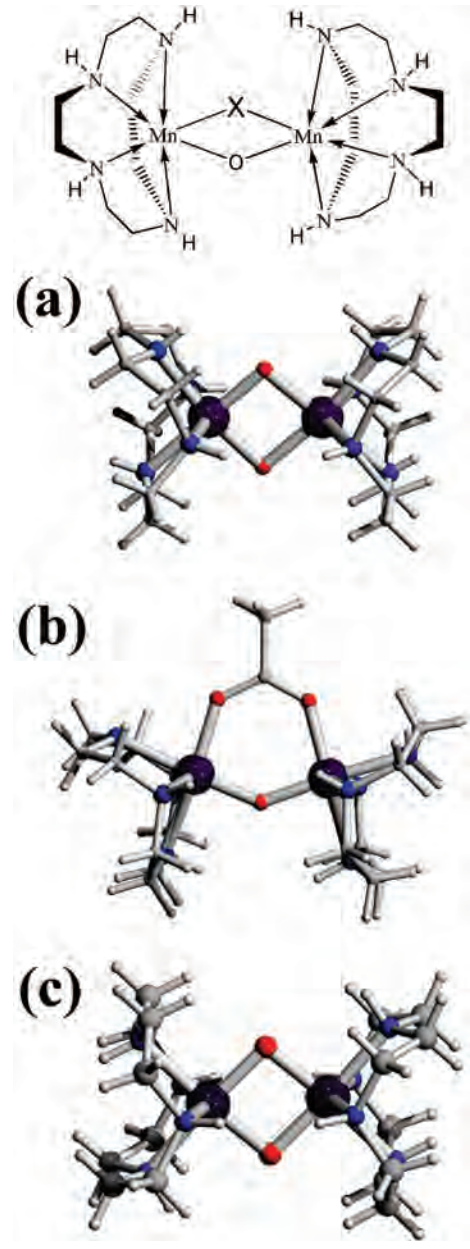

Figure 1. X-ray crystal structures of the dinuclear complexes of manganese with cyclen: (a) $[Mn_2(\mu_2\text{-}O)_2(C_8H_{20}N_4)_2]^{3+}$ (counteranions: $2Cl^-$, ClO_4^-), in **1** (X = O); (b) $[Mn_2(\mu_2\text{-}O)(\mu\text{-acetato})(C_8H_{20}N_4)_2]^{3+}$ (counteranion: $3ClO_4^-$), in **3** (X = acetato); (c) $[Mn_2(\mu_2\text{-}O)_2(C_8H_{20}N_4)_2]^{3+}$ in **2** and **4** (X = O).

(3) (a) Post, J. E. *Proc. Natl. Acad. Sci. U.S.A.* **1999**, *96*, 3447. (b) Roy, S. In *Manganese Materialization, Geochemistry and Minerology of Terrestrial and Marine Deposits*; Nicholson, J. R., Hein, J. R., Bühn, B., Dasgupta, S., Eds.; Special Publications; Geological Society: London, 1996, Vol. *119*, p 5. (c) Suib, S. L. In *Studies in Surface Science and Catalysis*; Chon, H., Woo, S. H., Park, S. E., Eds.; Elsevier: New York, 1996; Vol. *102*, pp 47−74. (d) *Synthesis, Properties and Applications of Oxide Nanomaterials*; Rodriguez, J. A., Ferdinandez-Garcia, M., Eds.; Wiley-Interscience: New York, 2007. (e) Sibbons, K. F.; Shastri, K.; Watkinson, M. *Dalton Trans.* **2006**, 645.

(4) Wu, A. J.; Pecoraro, V. L.; Penner-Hahn, J. E. *Chem. Rev.* **2004**, *104*, 903–938.

(5) (a) Brock, S. L.; Sanabria, M.; Suib, S. L.; Urban, V.; Thiyagarajan, P.; Potter, D. I. *J. Phys. Chem B* **1999**, *103*, 7416. (b) Yin, M.; O'Brien, S. *J. Am. Chem. Soc.* **2003**, *125*, 10180–10181.

(6) (a) Yang, X.; Makita, Y.; Liu, Z.; Sakane, K.; Ooi, K. *Chem. Mater.* **2004**, *16*, 5581. (b) Oaki, Y.; Imai, H. *Angew. Chem., Int. Ed.* **2007**, *46*, 4951.

(7) (a) Wang, L.; Ebina, Y.; Takada, K.; Sasaki, T. *Chem. Commun.* **2004**, 1074. (b) Chen, H.; He, J. *Chem. Lett.* **2007**, *36*, 174.

(8) Tian, Z.; Feng, Q.; Sumida, N.; Makita, Y.; Ooi, K. *Chem. Lett.* **2004**, *33*, 952.

(9) Tian, Z.; Tong, W.; Wang, J.; Duan, N.; Krishnan, V. V.; Suib, S. L. *Science* **1997**, *276*, 926.

(10) Hill, J. P.; Alam, S.; Ariga, K.; Anson, C. E.; Powell, A. K. *Chem. Commun.* **2008**, 383–385.

(11) (a) Wu, M.-S.; Chiang, P.-C. J. *Electrochem. Solid-State Lett.* **2004**, *7*, A123–A126. (b) Prasad, K. R.; Miura, N. *J. Power Sources* **2004**, *135*, 354–360. (c) Liu, P.; Lee, S.-H.; Yan, Y.; Tracy, C. E.; Turner, J. A. *J. Power Sources* **2006**, *158*, 659–662. (d) Cheng, F.; Zhao, J.; Song, W.; Li, C.; Ma, H.; Chen, J.; Shen, P. *Inorg. Chem.* **2006**, *45*, 2038–2044.

Figure 2. X-ray crystal structure of **2**.

coordination to the manganese centers. In **1**, six of the eight available amine groups are directed "inward" while the remaining two are directed "outward" from the center of the molecule. **2** and **4** have similar configurations of the amine groups: four situated above and below the plane of the Mn_2O_2 group are directed inward, while the other four are arranged in an alternating inward−outward configuration reminiscent of a fylfot cross[12] shortened along one axis. In the case of compound **3**, replacing one μ-oxo group with a μ-acetato group stabilizes an $Mn^{III}Mn^{III}$ oxidation state. **3** most commonly crystallizes as red needles, and the only hydrogen-bonding interaction involves the perchlorate counteranions. The structures of the dinuclear units in **1**, **2**, and **4** are similar to that of their cyclam analogue, which was originally studied by Calvin et al.[13]

In this work, we initially facilitated crystallization of the complexes using perchlorate (sodium salt) as an additive. For complex **1**, a single perchlorate counteranion is present hydrogen-bonded at one of the cyclen amine groups, but this perchlorate does not play a role in the extended structure. For the acetate-bridged complex **3**, perchlorate anions also do not play a significant structural role even in the absence of other counteranions. However, if sodium perchlorate was replaced with sodium isothiocyanate, complex **2** was obtained. The crystal structure of **2** is shown in Figure 2, which depicts the hydrogen-bonding interactions between the dinuclear unit and its counteranion (note that the dinuclear unit requires only one counteranion for charge balancing and that, in the figure, three other anions are included to illustrate the prevailing hydrogen-bond interactions). The counteranion is a pentacoordinate Mn^{2+} with isothiocyanate ligands, $[Mn(NCS)_5]^{3-}$. In this case, all cyclen amine groups are hydrogen-bonded to sulfur atoms of the $[Mn(NCS)_5]^{3-}$ counteranions so that two of the anions are hydrogen-bonded to three NH groups (one sulfur atom has two hydrogen bonds) and the remaining two are singly hydrogen-bonded. Disorder of one of the sulfur atoms of $[Mn(NCS)_5]^{3-}$ is apparently due to its being shared through hydrogen bonding with an amine group of an adjacent dinuclear unit. All hydrogen bonds are long, which is to be expected because sulfur is the acceptor in this case. This complex, containing an $Mn^{III}Mn^{IV}$ dinuclear unit and the $[Mn(NCS)_5]^{3-}$ counteranion, was obtained in admixture (mixture of different crystals) with the higher oxidation state $Mn^{IV}Mn^{IV}$ complex with $[Mn(NCS)_6]^{4-}$, although the crystal structure of this could not be properly refined. These isothiocyanate complexes were not studied further because of poor crystal quality and the mixture of products (further products of differing crystal habit were also produced).

An interesting feature of these dinuclear complexes presents itself when they are crystallized from solutions of manganese(II) oxalate, giving compound **4** (see Figure 3). The doubly oxo-bridged Mn^{III}/Mn^{IV} cyclen complex templates a quasi-one-dimensional manganese(II) oxalate, which has the form of infinite chains of edge-sharing six-membered rings. Not only does the dinuclear complex template the oxalate, it also acts as an isolating unit between adjacent chains, ensuring that they remain separated and avoiding the formation of a more usual templated two-dimensional network oxalate[14] (see Figure 3a,b). Templating is through hydrogen bonding between cyclen secondary amino groups and the oxygen atoms of the oxalate bridging ligands, as illustrated (Figure 3d). Dinuclear units template at two differing ("pillaring" and "separating") interchain sites, with the separating interchain unit displaying some disorder. The interchain templating dinuclear unit hydrogen bonds through cyclen amine groups to oxalate oxygen atoms at the edge of the oxalate chain (Figure 3e). The most obvious difference between the modes of templating of the dinuclear units is that the pillaring unit hydrogen bonds through the two amino groups of each cyclen ligand that lie coplanar with the plane of the Mn_2O_2 unit. The separating unit forms hydrogen bonds through the amino groups that lie above and below the Mn_2O_2 plane. Despite these differing hydrogen-bonding modes, the templates have similar conformations of their cyclen groups. The manganese(II) oxalate chains themselves are arranged parallel to the *b* axis. Neighboring chains are nearly coplanar, with a separation of the closest manganese atoms of 1.22 nm and a distance between centers of the chains of 2.23 nm. The oxalate chains are stacked in the direction of the *a* axis, with a separation of 0.95 nm between the planes of chains. This structuring is directed by the templating units, which also behave as interplane pillars. A significant number of disordered solvent (water and methanol) molecules is present in the interchain regions, but there are no solvent molecules in the intrachain regions. Compound **4** can thus, in some senses, be considered a hybrid material being comprised of an organometallic coordination complex templating an inorganic salt. One further interesting detail of this compound is the presence of manganese in three different oxidation states.

(12) Greg, R. P. *Archaeologia* **1885**, *48*, 298.
(13) Brewer, K. J.; Calvin, M.; Lumpkin, R. S.; Otvos, J. W.; Spreer, L. O. *Inorg. Chem.* **1989**, *28*, 4446–4451.
(14) (a) Tamaki, H.; Zhong, Z. J.; Matsumoto, N.; Kida, S.; Koikawa, M.; Achiwa, N.; Hashimoto, Y.; Okawa, H. *J. Am. Chem. Soc.* **1992**, *114*, 6974–6979. (b) Min, K. S.; Reingold, A. L.; Miller, J. S. *Inorg. Chem.* **2005**, *44*, 8433–8441.

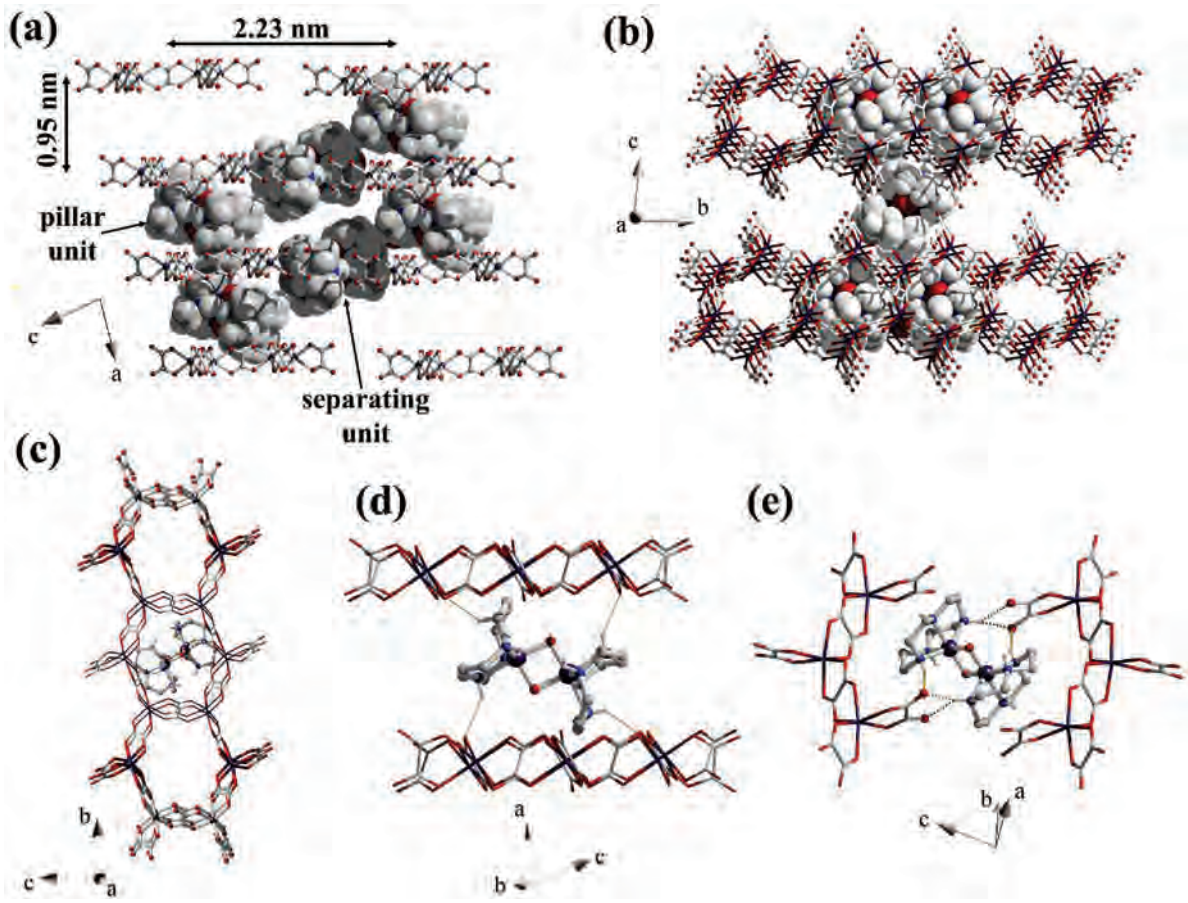

Figure 3. X-ray crystal structure of **4**. (a) View down the *b* axis. $[Mn_2(\mu_2\text{-}O)_2(C_8H_{20}N_4)_2]^{3+}$ units template chains of manganese(II) oxalate. A pillar unit separates planes of manganese(II) oxalate; the separating unit lies between chains. (b) View oblique to the *a* axis. Manganese(II) oxalate formed from edge-sharing macrocycles. Chains are stacked through a pillaring unit and divided by a separating unit. (c) View down the *a* axis. (d) Important hydrogen-bonding interactions between a pillaring unit and an oxalate chain. (e) Important hydrogen-bonding interactions between a separating unit and oxalate chains.

To summarize, the identity of the counteranions present in reaction mixtures of cyclen and manganese(II) salts has a substantial influence on the final crystal structures. This can be as subtle as a hydrogen-bonding interaction, leading to self-assembly of the dinuclear units into a sheet form (**1**), but can also entail sequestration of the manganese cations as a component of the species counteranionic to the dinuclear unit as in the cases of isothiocyanate (**2**) or oxalate (**4**). Although this variation of conditions is simple in principle, it permits increasing complexity in arriving at the hybrid templated manganese oxalate compound.

Electrochemistry. The previously unreported bimetallic Mn complex **3** exhibits two oxidations and two reductions within the accessible potential window of acetonitrile containing 0.1 M $(TBA)ClO_4$ (Figure 4a). The first anodic process located at $E_{1/2} = 0.93$ V vs Ag/AgCl involves a one-electron reversible oxidation as revealed by its peak-to-peak separation and scan rate dependence studies. A plot of the peak current versus the square root of the scan rate, for the data shown in Figure 4a inset, yielded straight lines for both anodic and cathodic peaks, indicating the electrochemical reversibility of this process.[15] Further, a metal-centered Mn^{III}/Mn^{IV} transition corresponding to this reversible oxidation is suggested by the spectroelectrochemical studies. That is, during the first oxidation, absorption bands at 280 and 495 nm due to the Mn^{III}/Mn^{III} complex decrease in intensity with the appearance of a new band at 715 nm (see Figure 4b) due to an oxo-to-Mn^{IV} charge transfer.[13] Absorption bands at 530 nm and one at 500 nm (which appears during oxidation) are likely due to d−d transitions localized at Mn^{III} and Mn^{IV}, respectively.[13] The second oxidation, located at $E_{pa} = 1.64$ V vs Ag/AgCl, was found to be irreversible, suggesting instability of the Mn^{IV}/Mn^{IV} species. Similarly, the two reductions located at $E_{pc} = -0.47$ and -1.38 V vs Ag/AgCl were found to be irreversible; hence, no further spectroelectrochemical studies were carried out. The overall redox behavior of **3** can be summarized as shown in Figure 4c. It should also be mentioned here that the acetato-bridged Mn^{III}/Mn^{III} form is unstable when dissolved in water, leading to the appearance of electronic absorption bands at 400, 550, and 650 nm consistent with the replacement of the bridging acetato with a bridging oxo ligand.[13]

Decomposition of Crystalline Products. Deep-green pristine crystals of **4** are only metastable under their mother liquor and are gradually redissolved with concurrent deposition of a black/brown solid over the period of several months. Reaction mixtures containing manganese(II) chloride or

(15) Bard, A. J.; Faulkner, L. R. *Electrochemical Methods: Fundamentals and Applications*, 2nd ed.; John Wiley: New York, 2001.

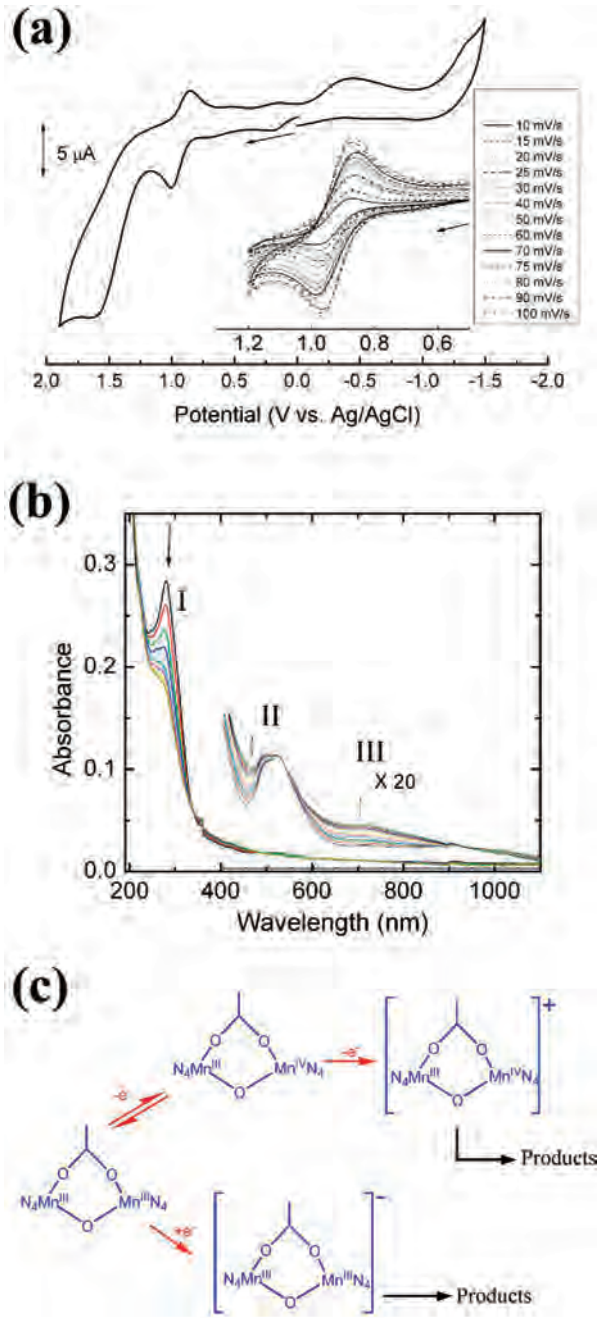

Figure 4. (a) Cyclic voltammogram of **3** in CH_3CN and 0.1 M tetra-*n*-butylammonium perchlorate at a scan rate of 100 mV s^{-1}. The inset shows the voltammograms corresponding to the first reversible oxidation at different scan rates. (b) Spectroelectrochemical changes during the first one-electron oxidation of **3** (I, ligand-to-metal charge transfer; II, d−d transitions; III, oxo-to-Mn^{IV} charge transfer). (c) Probable chemical changes occurring for **3** during reversible and irreversible redox processes.

manganese(II) acetate behave similarly. Morphologies of these black/brown solid products (labeled **1′**, **3′**, and **4′** for **1**, **3**, and **4**, respectively) are shown in Figure 5. For the $MnCl_2.4H_2O$ system, the product **1′** has the appearance of aggregated particles that are of a lamellar texture [see the field emission scanning electron microscopy (FE-SEM) image in Figure 5a] composed of MnO_2 with an organic intercalant.[10] Transmission electron microscopy (TEM; Figure 5b) confirms the lamellar structure and indicates a layer spacing around 2 nm. One hallmark of lamellar structures is that they can form tubular morphologies by rolling up of the lamellae. This is illustrated by the TEM image in Figure 5c, which shows a lamellar tube where the layer edges are clearly visible. This particular object may, in fact, be formed by rolling up of a single sheet into a hollow one-dimensional object by analogy with the cigar-rolling method.[16] The layered form of **1′** is in contrast to that exhibited by **3′** derived from the $Mn(CH_3CO_2)_2 \cdot 4H_2O$ reactions with cyclen (Figure 5d). Material deposited following crystallization of those solutions is a similar black/brown powder, but it is composed of a polynanocrystalline substance, as demonstrated by the high-resolution TEM (HR-TEM) image (Figure 5e). Crystal sizes are in the range 5−10 nm and are composed of MnO, as indicated by electron diffraction (ED) analysis (Figure 5f). Finally, **4′** exhibits a lamellar form and composition similar to **1′**, but it is contained in microspherical morphology (Figure 5g). TEM and HR-TEM imaging, including ED (Figures 5g−i), again illustrate the lamellar structure, and a layer spacing of 1.9 nm can be derived by analysis of these images. As previously reported, elemental and powder X-ray diffraction (XRD) analyses indicate that the lamellar materials are manganese oxides (MnO_2) containing various amounts of carbon and nitrogen.[10] To probe further the composition of the products from solution decomposition of **1**, **3**, and **4**, thermogravimetric analysis (TGA) was performed on **1′**, **3′**, and **4′**, and the result is shown in Figure 6 together with the TGA profile for crystals of compound **4**. For **4**, initial weight losses are due to solvents [methanol (50−60 °C) and then water (100−120 °C)], while the large weight loss above 350 °C can be attributed to decomposition of carboniferous materials. Thus, **1′**, **3′**, and **4′** are deficient in carbon compared to their precursors, which is consistent with the formation of the observed lamellar form of manganese oxide containing organic interstitial countercations. Finally, the addition of sodium perchlorate to reaction mixtures during the synthesis of **1** and **3** was for purposes of facilitating crystallization, and the synthesis of compound **4** requires no additive. Reaction mixtures lacking perchlorate can also end in the deposition of lamellar-structured products for **1**, so that the perchlorate reagent is not required for the preparation of the materials described here. However, crystallization of compounds **1** and **3** permitted identification of the initial species involved in this system.

In order to assess the effect of removing the organic components from **1′**, **3′**, and **4′**, SEM analyses were performed on samples after heating at 600 °C under a nitrogen atmosphere. This revealed that the morphology is to some extent maintained for **1′** and **4′**, while for **3′**, there is not a significant change in the appearance of the sample (Figure 7). We suggest for **3′** that the organic portion of the material forms a matrix for the nanocrystalline material and is not an intimate part of the structure so that its removal does not substantially alter the form of the sample. On the other hand, the organic components of **1′** and **4′** should be

(16) (a) Ma, R.; Bando, Y.; Sasaki, T. *J. Phys. Chem. B* **2004**, *108*, 2115–2119. (b) Wang, F.; Jiu, J.; Pei, L.; Nakagawa, K.; Isoda, S.; Adachi, M. *Chem. Lett.* **2005**, *34*, 1238–1239.

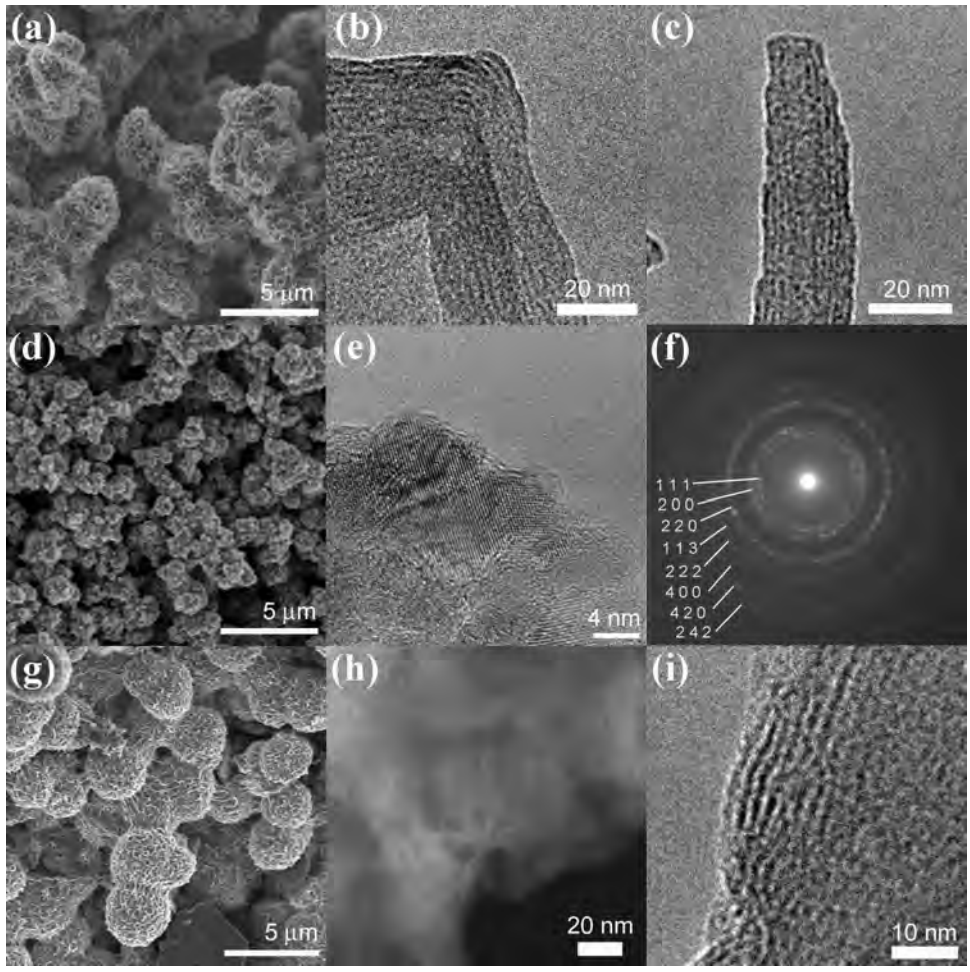

Figure 5. Electron microscopy of the materials **1′**, **3′**, and **4′** derived from decomposition of **1**, **3**, and **4**. (a) SEM of **1′**. (b) HR-TEM of **1′** showing lamellar features. (c) Tubular structure formed by the rolling up of layers of **1′**. (d) SEM of **3′**. (e) HR-TEM of **3′** indicating the nanocrystalline structure. (f) ED pattern at a polycrystalline region of **3′**, with indexing indicating its identity as MnO. (g) Nanostructured microspheres derived from decomposition of **4**. (h) Dark-field scanning transmission electron microscopy (STEM) image of **4′**. (i) HR-TEM image of **4′** revealing its lamellar structure.

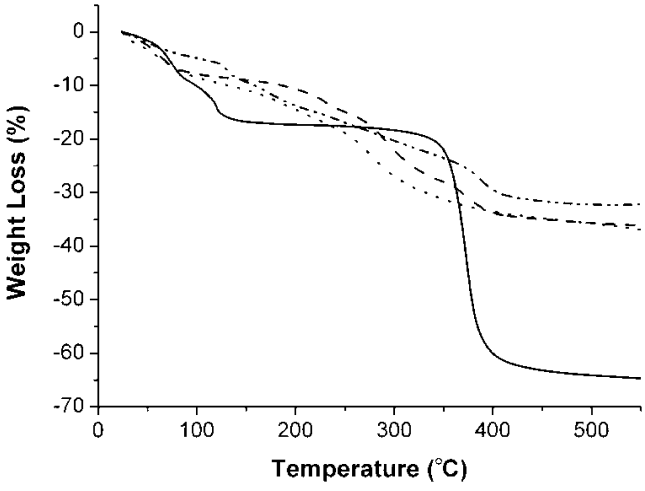

Figure 6. TGA of **4** (—), **1′** (− −), **3′** (•••), and **4′** (-••-).

intercalated in the lamellar structure. Thermolysis of **1′** or **4′** does result in changes to the morphologies of the samples. At low magnification (∼5000×), the samples still appear to possess a layered structure, but when observed more closely, the spongelike structures can be seen to be composed of particles 30−40 nm in diameter. The lamellar form of samples **1′** and **4′** has been imprinted onto the final particulate structure.

Previously, thermolysis of coordination complexes has been used as a method for the preparation of materials of certain composition or for obtaining nanostructured products.[17] In this case, we thermolyzed compound **4** because its extended one-dimensional structure and high manganese content suggested the possibility of obtaining novel nanostructured products. When **4** was subjected to thermolysis at 600 °C under nitrogen or air atmospheres, various products could be obtained. When thermolysis was performed by heating under nitrogen at 600 °C, the main product observed by powder XRD was manganese oxide, MnO (as expected for manganese(II) oxalate[18]), while under air, the corresponding product was Mn_2O_3, apparently contaminated with small (∼1 wt %) amounts[18] of other oxides including Mn_3O_4. The formation of Mn_2O_3 might be explained by supposing that thermal decomposition of the cyclen ligand implies loss of more oxidizing equivalents from the complex, thus maintaining manganese in a lower oxidation state than that

(17) Schmitt, W.; Hill, J. P.; Malik, S.; Volkert, C. A.; Ichinose, H.; Anson, C. E.; Powell, A. K. *Angew. Chem., Int. Ed.* **2005**, *44*, 7048.
(18) Ahmad, T.; Ramanujachary, K. V.; Lofland, S. E.; Ganguli, A. K. *J. Mater. Chem.* **2004**, *14*, 3406–3410.

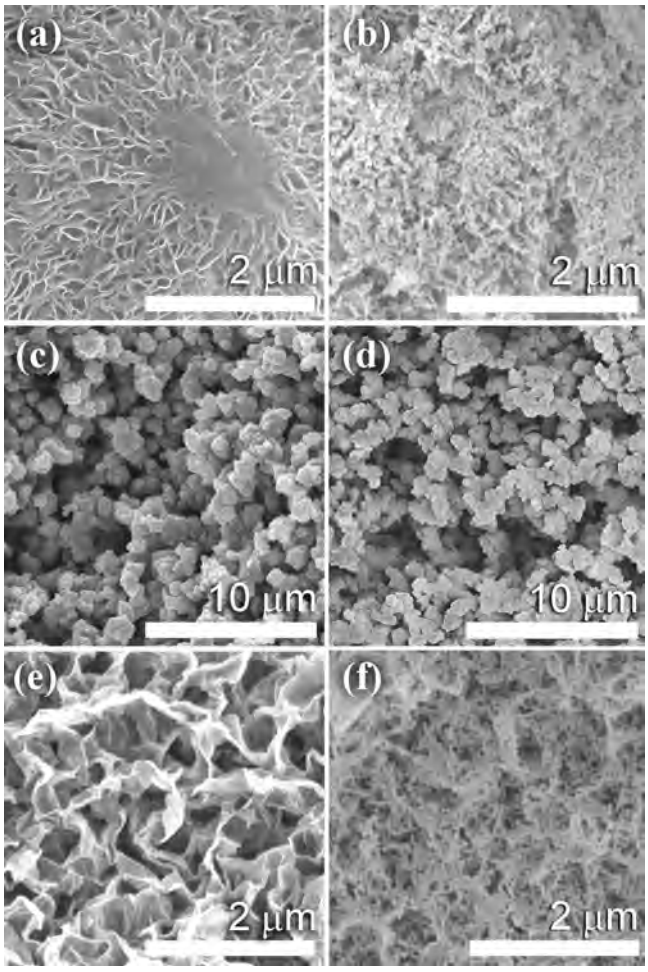

Figure 7. SEM images of **1′** (a), **3′** (c), and **4′** (e) and the products of their pyrolysis, parts b, d, and f, respectively.

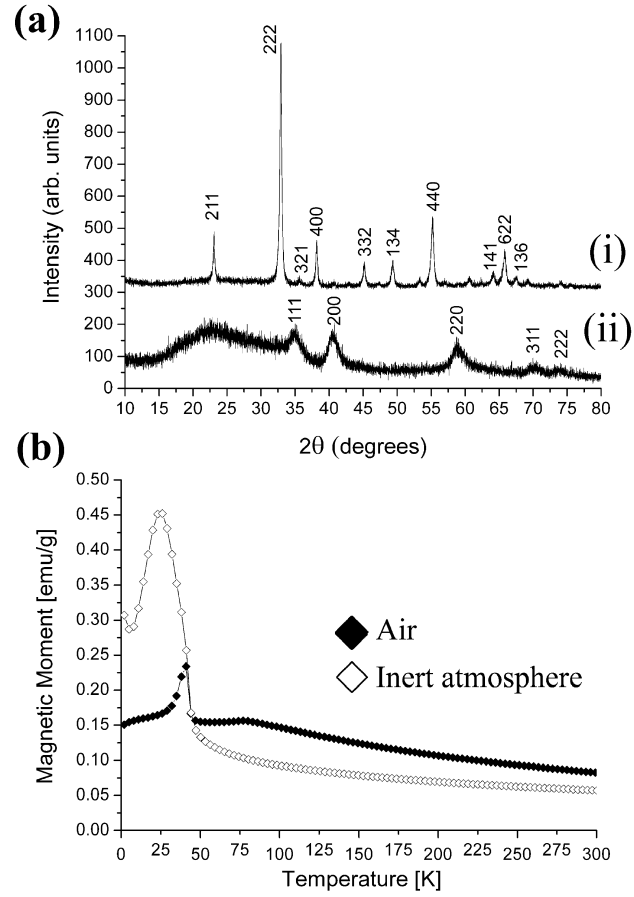

Figure 8. (a) Powder X-ray diffractograms and (b) temperature dependencies of magnetic moments of the products of pyrolyzing **4** under an air or inert (dinitrogen) atmosphere. In part a(ii), the broad peak around $2\theta = 20°$ is due to the background.

expected for thermolysis of manganese(II) oxalate in air, which usually gives Mn_3O_4.[18] The powder XRD patterns of the products obtained from compound **4** are shown in Figure 8a, while temperature dependencies of their magnetic moments are shown in Figure 8b. Clearly, while Mn_2O_3 and MnO appear to be the main products, both materials contain Mn_3O_4, indicated by the transition around 45 K. The lack of signals due to Mn_3O_4 in XRD might be due to the presence of Mn_3O_4 only at the particles' surfaces[19] (or alternatively to line broadening or lack of crystallinity), and only small (~1 wt %) amounts of this contaminant would be necessary to obtain the observed response in the magnetic property. For the sample prepared by heating in air, the feature close to 80 K is characteristic of Mn_2O_3.[18]

The reaction for the preparation of complex **1** can be scaled, and it is convenient for developing methods to obtain the lamellar nanostructured manganese oxide either in larger quantities or for deposition on a suitable substrate. In those cases, the synthesis was performed without the addition of the crystallization facilitator sodium perchlorate. Under these conditions, the solutions normally deposit the nanostructured product directly without leading to a crystalline product. If a substrate such as a section of silicon wafer or an indium−tin oxide (ITO) glass plate was also inserted in the reaction mixture, then deposition also occurred at the substrate surface. SEM images of the resulting structures are shown in Figure 9. Coverage of the substrate could be controlled by variation of the immersion time as indicated. At low-to-medium coverage, the structures are stable upon removal from the supernatant. However, when coverage becomes more complete (i.e., a film is formed), removal from the solution results in peeling of the film from the substrate during shrinkage caused by drying in air. Films are reasonably stable if maintained in a wet state. An interesting result of the peeling process is that it can lead to the formation of a thin film of even thickness on the substrate surface. As shown in parts c and d of Figure 9, during peeling, cleavage of the thick film occurs, resulting in a residual film of around 1 μm, which possesses improved homogeneity of thickness. This peel-back method could be of use for the preparation of evenly functionalized electrodes, although it is currently a rather atom-inefficient process, with the bulk of the nanostructured product formed being discarded as the peeling layer.

Conclusion

In summary, we have prepared dinuclear complexes of Mn^{III}/Mn^{IV} with the macrocyclic ligand 1,4,7,10-tetraazacyclododecane. Of particular note is the one-dimensional

(19) Butler, G.; Thirsk, H. R. *Acta Crystallogr.* **1952**, *5*, 288–289.

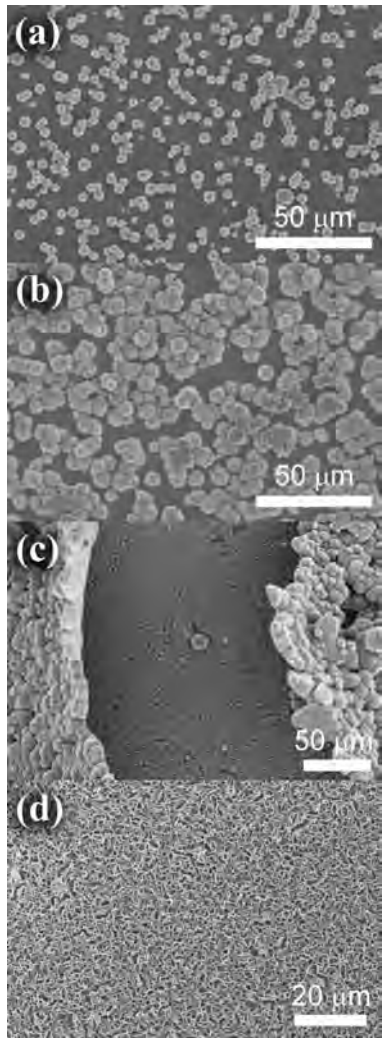

Figure 9. Growth of nanostructured films at surfaces. (a) Low coverage (~30%) of decomposed **1** on passivated silicon (2−3 days). (b) Higher coverage where growth has begun on top of the existing growth (1−2 weeks). (c) Thick film peeling from the surface, giving a ~1-μm-thick layer. (d) Homogeneous film resulting from peeling.

oxalate of manganese(II) derived from templating by one of the dinuclear complexes, which can be considered a hybrid oxalate material. Electrochemical and spectroelectrochemical studies of the oxo-acetato-bridged complex **3** revealed reversible cycling between Mn^{III}/Mn^{III} and Mn^{III}/Mn^{IV} under the appropriate conditions; however, further oxidation and reduction were found to be irreversible. Decomposition of the complexes using wet routes or by thermolysis is a valid means to obtain nanostructured Mn-containing materials. The lamellar materials resulting from the use of wet routes are suitable for processing such as, for instance, catalysts and can be grown on substrates, notably silicon oxide or ITO glass. Thick (>5 μm) films of the latter materials were found to be less stable, undergoing peeling from the substrates. However, this peeling process resulted in the formation of thin films with improved homogeneity of thickness due to cleavage occurring during the peeling of the thick film from the substrate surface. We are currently undertaking an in-depth study in order to determine the effect of the transition-metal identity on the structures and properties of the respective products. Finally, we are investigating the utility of the peel-back process for the preparation of electrochemically active films.

Experimental Section

All solvents and reagents were purchased from commercial sources (Aldrich Chemical Co., Lancaster Chemical Co., and Riedel-de-Häen) and used as received. 1,4,7,10-Tetraazacyclododecane (cyclen) was purchased from Strem Chemical Co. Manganese(II) oxalate was prepared by a literature method.[20] Compound **1** was prepared as previously described.[10] Complex **2** was prepared by the same method as that given for **1** but excess sodium isothiocyanate was added to the reaction mixture rather than sodium perchlorate. Mixtures of products from reactions leading to complex **2** precluded a reliable chemical analysis. Samples for elemental analysis were dried overnight in a vacuum prior to measurement.

Syntheses. 3. Cyclen (0.1 g, 5.8×10^{-4} mol) dissolved in methanol (20 mL) was added dropwise to a stirred solution of manganese(II) acetate (0.142 g, 1 equiv, 5.8×10^{-4} mol) in methanol (20 mL), and the mixture was stirred for 5 min before the addition of sodium perchlorate (0.5 g). The solution was filtered and allowed to stand in an open flask overnight. The resulting long red needlelike crystals of **2** were filtered and washed sparingly with methanol. FT-IR (KBr): δ 3439.1 (br, m), 3320.1 (m), 3243.2 (br, m), 2937.4 (m), 2887.8 (m), 1627 (w), 1533.7 (m), 1443.2 (m), 1108.8 (s), 1004.1 (m), 985.0 (m), 930.5 (w), 912.3 (w), 865.8 (w), 802.2 (m), 669.8 (w), 636.4 (w), 625.2 (m), 558.5 (w), 517.1 (w), 447.6 (w) cm^{-1}. Elem anal. Found: C, 25.94; H, 5.31; N, 12.74. Calcd for $C_{18}H_{43}Cl_3Mn_2N_8O_{15}$: C, 26.09; H, 5.19; N, 13.53.

4. Cyclen (0.1 g, 5.8×10^{-4} mol) was added to a suspension of manganese(II) oxalate dihydrate (0.105 g, 1 equiv, 5.8×10^{-4} mol) in water (20 mL). The resulting cloudy solution was allowed to stir at room temperature during dissolution of the manganese oxalate and then filtered, and methanol (5−6 mL) was slowly added. The solution was filtered and allowed to stand in a flask covered with perforated parafilm. After 2−3 days, large dark-green parallelepipeds suitable for crystallography had formed. FT-IR (KBr): δ 3436.4 (br, s), 3225.1 (br, s), 2934.1 (m), 2883.1 (m), 1610.1 (s), 1456.5 (m), 1436.7 (m), 1315.5 (s), 1182.8 (w), 1087.5 (m), 1056.2 (m), 1012.7 (w), 989.5 (w), 956.1 (w), 864.1 (w), 794.4 (m), 696.0 (m), 667.9 (w), 645.1 (w), 498.7 (w) cm^{-1}. Elem anal. Found: C, 30.23; H, 4.66; N, 12.21. Calcd for $C_{46}H_{80}Mn_8N_{16}O_{32}$: C, 30.53; H, 4.42; N, 12.39.

Nanostructured MnO_2 Synthesis. In the case of reactions leading to compound **1**, sodium perchlorate was not added to the reaction mixture during synthesis, and lamellar forms of manganese oxides were gradually deposited. For compounds **3** and **4**, the crystals were allowed to stand under the supernatant, leading gradually to deposition of nanostructured microparticles. Films of the nanomaterial derived from **1** deposited on silicon wafer or glass substrates were prepared by immersion of the selected substrate in an aqueous solution of **1** and standing for the appropriate time period (typically 2−3 weeks).

Electrochemistry. Cyclic voltammograms were recorded on an EG&G model 263A potentiostat using a three-electrode system. A platinum button or glassy carbon electrode was used as the working electrode. A platinum wire served as the counter electrode, and Ag/AgCl was used as the reference electrode. Spectroelectrochemical studies were performed on a homemade thin-layer optical cell using the three-electrode configuration. All solutions were purged using an argon gas prior to electrochemical and spectral measurements.

(20) Coltman, R. W. *Ind. Eng. Chem.* **1924**, *16*, 606–609.

X-ray Crystallography. 1.[10] $C_{64}H_{40}Cl_3Mn_2N_8O_6$, fw 656.79 g mol^{-1}, orthorhombic, *Pnma*, a = 22.3850(14) Å, b = 9.1934(5) Å, c = 13.2424(10) Å, V = 2725.2(3) Å^3, T = 200 K, $F(000)$ = 1364, ρ_{calc} = 1.601 Mg m^{-3}, μ(Mo Kα) = 1.267 m^{-1}, Stoe IPDS diffractometer, λ = 0.710 73 Å, 15 645 data measured to $2\theta_{max}$ = 52°, of which 2709 were unique (R_{int} = 0.1230), structure solution by direct methods and full-matrix refinement against F^2 (all data) using *SHELXTL*,[21] 192 parameters, final wR2 = 0.0903, S = 0.967 (all data), R1 = 0.0480 [1397 with $I > 2\sigma(I)$].

2. $C_{21}H_{40}Mn_3N_{13}O_2S_5$, fw 831.78 g mol^{-1}, monoclinic, *I*2/*a*, a = 18.2699(10) Å, b = 11.2384(6) Å, c = 18.6432(9) Å, α = 90.00°, β = 114.510(6)°, γ = 90.00°, V = 3483.0(3) Å^3, T = 200 K, $F(000)$ = 1712, ρ_{calc} = 1.586 Mg m^{-3}, μ(Mo Kα) = 1.413 m^{-1}, Stoe IPDS diffractometer, λ = 0.710 73 Å, 17 817 data measured to $2\theta_{max}$ = 52°, of which 3195 were unique (R_{int} = 0.0839), structure solution by direct methods and full-matrix refinement against F^2 (all data) using *SHELXTL*,[21] 213 parameters, final wR2 = 0.1425, S = 1.092 (all data), R1 = 0.0536 [2903 with $I > 2\sigma(I)$].

3. $C_{18}H_{43}Cl_3Mn_2N_8O_{15}$, fw 827.83 g mol^{-1}, orthorhombic, *Pca*21, a = 13.9322(11) Å, b = 16.2332(13) Å, c = 14.6794(8) Å, V = 3320.0(4) Å^3, T = 200 K, $F(000)$ = 1712, ρ_{calc} = 1.656 Mg m^{-3}, μ(Mo Kα) = 1.079 m^{-1}, Stoe IPDS diffractometer, λ = 0.710 73 Å, 15 645 data measured to $2\theta_{max}$ = 52°, of which 6267 were unique (R_{int} = 0.0483), structure solution by direct methods and full-matrix refinement against F^2 (all data) using *SHELXTL*,[21] 435 parameters, final wR2 = 0.0838, S = 0.963 (all data), R1 = 0.0477 [3059 with $I > 2\sigma(I)$].

4. $C_{46}H_{117}Mn_8N_{16}O_{50.5}$, fw 2142.08 g mol^{-1}, triclinic, $P\bar{1}$, a = 9.5442(11) Å, b = 10.3758(10) Å, c = 21.851(2) Å, α = 83.720(12)°, β = 80.106(13)°, γ = 85.457(13)°, V = 2114.9(4) Å^3, T = 200 K, $F(000)$ = 1109, ρ_{calc} = 1.682 Mg m^{-3}, μ(Mo Kα) = 1.263 m^{-1}, Stoe IPDS diffractometer, λ = 0.710 73 Å, 12 685 data measured to $2\theta_{max}$ = 52°, of which 7554 were unique (R_{int} = 0.0513), structure solution by direct methods and full-matrix refinement against F^2 (all data) using *SHELXTL*,[21] 558 parameters, final wR2 = 0.1049, S = 0.967 (all data), R1 = 0.0498 [3821 with $I > 2\sigma(I)$].

Magnetic Susceptibility. Magnetic susceptibility measurements were carried out on a Quantum Design 5T MPMS.

Electron Microscopy. SEM (Hitachi S-4600) was performed on platinum-coated samples (~5 nm, Hitachi E-1030 ion sputterer) deposited on silicon substrates. Accelerating voltages were typically 4 keV. TEM was performed on a JEOL 2100F equipped with STEM and EDX facilities and operating at 200 keV (HR-TEM mode) or 100 keV (STEM mode). Samples were mounted on carbon-coated copper grids.

Acknowledgment. This work was supported by the World Premier International Research Center Initiative (WPI Initiative), MEXT, Japan. This work was also supported by a Grant-in-Aid for Science Research in a Priority Area "Super-Hierarchical Structures" from the Ministry of Education, Culture, Sports, Science and Technology, Japan, and National Science Foundation (Grant 0453464 to F.D.). This work was supported by the DFG-funded Center for Functional Nanostructures. The authors express their thanks to T. Sasaki (NIMS) and Dr. S. Acharya (NIMS) for performing the TEM and HR-TEM measurements and to Dr. M. Higuchi (NIMS) for use of the thermal analysis equipment. The authors would also like to thank Dr. Ajayan Vinu (NIMS) for helpful discussions.

Supporting Information Available: X-ray crystallographic files in CIF format. This material is available free of charge via the Internet at http://pubs.acs.org.

IC8008915

(21) Sheldrick, G. M. *SHELXTL 5.1*; Bruker AXS Inc.: Madison, WI, 1997.